Applied Catalysis B: Environmental 132–133 (2013) 499–510

Contents lists available at SciVerse ScienceDirect

Applied Catalysis B: Environmental

journal homepage: www.elsevier.com/locate/apcatb

Effect of Ce/Zr ratio in CeZr-CoRh catalysts on the hydrogen production by glycerol steam reforming

L.M. Martínez T[a], M. Araque[a,b], J.C. Vargas[b], A.C. Roger[a,*]

[a] Laboratoire des Matériaux, Surfaces et Procédés pour la Catalyse LMSPC, équipe "Energie et Carburants pour un Environnement Durable", UMR CNRS 7515, ECPM–Université de Strasbourg, 25 rue Becquerel, 67087 Strasbourg Cedex 2, France

[b] Departamento de Ingeniería Química y Ambiental, Universidad Nacional de Colombia Ciudad Universitaria, Avenida Carrera 30 No. 45-03, Edificio 453, Bogotá D.C., Colombia

ARTICLE INFO

Article history:
Received 31 July 2012
Received in revised form
11 December 2012
Accepted 13 December 2012
Available online 27 December 2012

Keywords:
Glycerol
Hydrogen production
Steam reforming
Mixed oxides
Rhodium catalysts
Cobalt catalysts
Glycerol decomposition

ABSTRACT

The H_2 production by glycerol steam reforming has been studied using fluorite-type mixed oxides of CZCoRh. The effect of the Ce/Zr ratio on the catalytic properties and its influence on the catalytic behavior are discussed. The catalysts were characterized before and after catalytic test by XRD, Raman spectroscopy, BET surface area, HRTEM, H_2-TPR and TPD-TPO. The results show that an increase of the cerium amount enhances both the stability and the selectivity toward H_2 and CO_2. This is related to the improvement of the reducibility and re-oxidation properties, oxygen storage capacity and metal support interaction. The activity results demonstrate that selective H_2 production is related to the capacity of the catalysts to activate H_2O under reaction conditions. This step ensures the steam reforming of the by-products to H_2. The progressive loss of this capacity reduces the H_2 production, decreasing the steam reforming ability and the glycerol decomposition becomes predominant. In this last case the production of CO, CH_4 and C_2H_4 is promoted along with the formation of condensable products as hydroxyacetone, acetaldehyde and acrolein.

1. Introduction

The production of hydrogen by glycerol steam reforming is an alternative to valorizing the glycerol originated from the biodiesel production as well as an alternative for H_2 production from the residual fraction of soap manufacture and lignocelluloses-to-ethanol conversion [1]. Glycerol steam reforming occurs according to the following chemical reaction [2]:

$$C_3H_8O_3 + 3H_2O \rightarrow 3CO_2 + 7H_2 \quad (\Delta H^\circ_{298} = +123\,kJ/mol)$$

Catalytic steam reforming must be carried out at high temperature, low pressure and high steam to glycerol ratio to achieve higher conversions [1,3,4]. In our previous study [5] it was found that H_2 production by glycerol steam reforming was optimal at temperatures higher than 650 °C, water/glycerol ratio of 9:1 and atmospheric pressure.

In addition to the experimental conditions, the use of appropriate catalysts also determines the good selectivity and stability toward H_2 and CO_2 production. The catalyst should involve the preferential cleavage of C—C bonds as opposed to C—O bond to increase the H_2, CO_2 and CO productions [6,7]. Furthermore, since the decomposition of glycerol is highly favorable, the catalyst must have sufficient capacity to reform the intermediate adsorbed species into hydrogen and carbon monoxide, and it must also facilitate the water gas shift reaction (WGS) to convert CO and H_2O into CO_2 and H_2 [8–13]. All these conditions are required to decrease the deactivation of the catalysts due to a sever carbon deposition [3].

Ceria based catalysts are well known for their *redox* properties and therefore for their high performance in WGS reaction [14,15]. It is known that the introduction of zirconium enhances oxygen mobility even further, improving the *redox* properties and the oxygen buffering action observed for the Ce oxides [13]. Ceria–zirconia (CZ) mixed oxides are also thermally stable and the oxygen storage capacity is retained even after many consecutive cycles of reduction at high temperature followed by re-oxidation [15]. These properties improve even more the catalytic activity in oxidation, reforming and WGS reactions [16,17].

Different works in steam reforming reactions have been carried out using cobalt [18,19] and nickel [20] on CZ supports. The strong metal-support interaction reached with such mixed oxide catalysts enhances the catalytic behavior [17]. However, the product distribution in gaseous phase change with time on stream showing deactivation related to the formation of carbonaceous deposits. In an attempt to reduce the deactivation of catalysts by carbon

* Corresponding author.
E-mail address: annececile.roger@unistra.fr (A.C. Roger).

0926-3373/$ – see front matter © 2013 Elsevier B.V. All rights reserved.
http://dx.doi.org/10.1016/j.apcatb.2012.12.027

formation it has been proposed to add small quantities of noble metals to the mixed oxide catalysts [1,21–23]. The addition of small amounts of Rh improves the stability of the cobalt catalysts suppressing the formation of carbonaceous deposits [20] by the powerful nature of Rh in breaking the C—C bonds [24].

The CZ mixed oxides with Co and/or Rh have been widely studied in our research group for steam reforming of ethanol [25], isooctane [26] and glycerol [5,27]. It has been proven by XANES that cobalt can be, by an appropriate method of synthesis, inserted under the form of Co^{2+} in octahedral coordination, modifying the local environment of Ce^{4+} and Zr^{4+}cations and favoring the reducibility, activity and stability of the catalysts [28]. However, the incorporation of both Co and Rh to CZ has favored even more the activity and selectivity toward H_2 by the strong metal-support interaction originated. Consequently both metals diminish the formation of carbonaceous deposits thanks to a cooperative metal–metal effect. The introduction of Rh favors the *redox* properties of the mixed oxides promoting the reduction of both Co and support, enhancing the oxygen storage capacity and also promoting the gasification of carbon deposited. Furthermore Rh can stabilize Co in the oxide matrix, avoiding its rejection as Co_3O_4 [27].

Our contribution with this study to the knowledge of CZCoRh catalysts for glycerol steam reforming is to show the effect of the Ce/Zr ratio on the physico-chemical properties of mixed oxide catalysts and its influence on the improved catalytic response toward higher selectivity of H_2. The structural and textural properties, *redox* behavior, oxygen storage capacity, metal support interaction and resistance to carbon deposition were determined by the combination of several characterization techniques as XRD, Raman spectroscopy, BET analysis, HRTEM, H_2-TPR, re-oxidation capacity and TPD-TPO. The possible causes of deactivation are discussed after the characterization of the spent catalysts and the analysis of formed by-products. The influence of the ceria amount on the reforming capability of the catalysts is presented and related to the physico-chemical properties of the materials.

2. Experimental

2.1. Preparation of the catalysts

The catalysts have been synthesized using the pseudo sol–gel method based on thermal decomposition of metallic propionates [19,20]. The salts used for the synthesis were cerium (III) acetate hydrate, zirconium (IV) acetylacetonate, cobalt (II) acetate and rhodium (II) acetate supplied by Aldrich. First of all, they were dissolved separately in propionic acid at a concentration of 0.12 mol l^{-1}. Then, the solutions were mixed and the solvent was evaporated until a resin was obtained. Finally, the resin was heated at 2 °C min^{-1} from room temperature to 700 °C and was maintained at this temperature for 6 h. Three catalysts were prepared with different Ce/Zr ratios: $Ce_{0.53}Zr_{2.97}Co_{0.47}Rh_{0.03}O_{8-\delta}$ with a *Poor* content of ceria (CZ^{P}CoRh; 0.20/0.80 CeO_2/ZrO_2 mass ratio); $Ce_2Zr_{1.5}Co_{0.47}Rh_{0.03}O_{8-\delta}$ with an *Intermediate* content of ceria (CZ^{I}CoRh; 0.65/0.35 CeO_2/ZrO_2 mass ratio); and $Ce_{2.59}Zr_{0.91}Co_{0.47}Rh_{0.03}O_{8-\delta}$ with a *Rich* content of ceria (CZ^{R}CoRh; 0.80/0.20 CeO_2/ZrO_2 mass ratio).

2.2. Catalytic tests

Glycerol steam reforming was performed in a conventional 30 cm straight tubular quartz reactor (ID = 7 mm) at atmospheric pressure for 24 h. The description of the home-made rig has already been reported [5]. The reaction was performed using 55 mg of catalysts diluted with 55 mg of silica carbide (SiC - supplied by SICAT®). Before the catalytic reaction, the catalysts were reduced with 3 ml min^{-1} of pure H_2 for 12 h at 450 °C using 2 °C min^{-1}. After reduction, the remaining H_2 was flushed out of the system using a 31 ml min^{-1} of N_2:Ar gas flow (1:4 molar ratio). Simultaneously, the temperature was increased up to the reaction temperature (650 °C) at 2 °C min^{-1}. The reactant solution was a mixture of glycerol (SIGMA ALDRICH 99.0%) and deionized water with 1:9 molar ratio. It was pumped into the system using a Gilson 350 micro pump and introduced into the reactor using a dosage device. The reactant liquid flow (0.0213 g min^{-1}), equivalent to 19 ml min^{-1} gas flow (STP), was diluted with the N_2:Ar gas flow. N_2 was used as internal standard for the quantification of non-condensable products. The experimental runs were conducted at space velocity of 8.4 $g_{glycerol}$ $g_{catal.}^{-1}$.

For the regeneration test three cycles of glycerol steam reforming were performed using CZ^{R}CoRh at regular conditions. After each cycle, the feed flow (glycerol:water) was stopped and 30 ml min^{-1} of air were introduced. The temperature of oxidation was fixed at the reaction temperature (650 °C), and the catalyst was maintained under these conditions for 4 h. After oxidation, the air flow was flushed out of the reactor with argon, and the catalyst was re-reduced at 450 °C with 3 ml min^{-1} of pure H_2 for 12 h (usual protocol).

The reaction products were divided and quantified separately. The non-condensable products (H_2, CO, CO_2, CH_4, C_2H_4) were characterized by on-line gas chromatography every 30 min using a Carbosieve II column. The condensable products were recovered by two traps: the first one at room temperature and the second one at 0 °C. The recovery was done after 5, 8.5 and 24 h of reaction. The products were analyzed by gas chromatography using a ZB-Wax Plus (Zebron) column with n-propanol as internal standard. The condensable products analyzed were acetone, acetaldehyde, acroleine, methanol, ethanol, hydroxyacetone, acetic acid, propionic acid, propyleneglycol, ethyleneglycol, glyceraldehyde and glycerol.

The analytical method used to determine the catalytic performance of the catalysts has already been reported [27]. Global conversion of glycerol (X) was calculated from the glycerol recovered from the condensable phase. Besides this, the conversions to non-condensable (X_G) and condensable products (X_L) were also determined. The conversion values of Figs. 8 and 12B are expressed as weighted mean with time taking into account the reaction time selected to recover the condensable products.

2.3. Catalysts characterization

- The crystalline structure of the mixed oxides catalysts was determined by XRD in a Brucker AXS-D8 Advanced equipment with Cu Kα radiation (λ = 1.5404 Å). The 2θ range scanned was from 10° to 90° with a 0.05° step size at a scan rate of 3 min^{-1}. All the results were confirmed by the crystalline structure we use the database.
- Raman Spectroscopy measurements were recorded in a dispersive Horiva Jobin Yvon LabRam HR800 Microscope, with a He—Ne green laser (532.14 nm) working at 5 mW, and with a 600 g mm^{-1} grating. The microscope used a 20× objective and a confocal pinhole of 150 μm. The Raman spectrometer is calibrated using a silicon wafer. Two types of measures were performed: (i) at room temperature under inert atmosphere and (ii) cycles of reduction-re-oxidation using pure H_2 and synthetic air. For the latter a Linkam CCR100 cell was used coupled to the Raman equipment. The temperature was increased from room temperature until 550 °C at 10 °C min^{-1}. The spectra were taken each 100 °C after 15 min of stabilization.
- Specific surface areas were determined by nitrogen physisorption measurements at 77 K (Brunauer–Emmett–Teller, BET method)

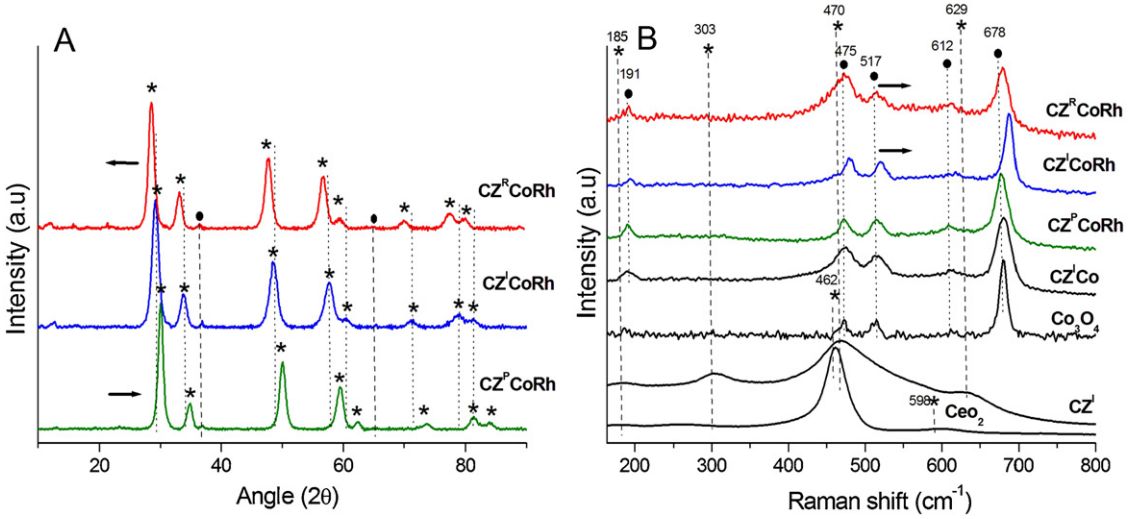

Fig. 1. (A) X-ray diffractograms and (B) Raman spectra at room temperature for fresh catalysts. Symbols: (*) CZ oxide and (●) Co_3O_4 spinel.

using a COULTER SA 3100 equipment. Prior to the analysis, the samples were out gassed at 250 °C for 16 h.

- High resolution transmission electron microscopy (HRTEM) observations were carried out with a TOPCON EM-002B apparatus (accelerating voltage 200 kV), which was coupled to an EDS KEVEX Deltapro Quantum for EDXS measurements. Before analysis, the samples were dispersed in toluene. TEM-EDXS analyses were performed with different probe sizes: 200 nm for global measurements (G), and probe sizes between 8.8 and 14.4 nm for local measurements (1–6 points).
- H_2-TPR were carried out in a Micromeritics AutoChem II 2920 equipment with a TCD detector. The analyses were performed on 30 mg of fresh catalyst under 50 ml min^{-1} of a 10% H_2/Ar mixture. The temperature was increased from room temperature to 1000 °C at 15 °C min^{-1}. The total H_2 consumption and the percentage of cerium reduced were calculated from the integration of TPR results. The H_2 consumption was discriminated by regions at low (25–550 °C) and high (550–1000 °C) temperatures, and the corresponding percentage were calculated with respect to the global consumption. The percentage of reduced cerium (Ce^{4+} to Ce^{3+}) was determined assuming a total reduction of Co_3O_4 to Co^0 and Rh_2O_3 to Rh^0 [25].
- TPD-TPO analyses were carried out in a Micromeritics AutoChem II 2920 equipment. The products were followed by mass spectrometry using an Omnistar TM equipment. 20 mg of spent catalyst were submitted to 50 ml min^{-1} of pure He for the desorption; and to 50 ml min^{-1} of 10% O_2 diluted in He for the oxidation. The temperature was increased to 1000 °C at 15 °C min^{-1}. The m/z signals 16, 18, 28, 32 and 44 were registered. However, only the results of the *m*/*z* 44 (CO_2 signal) are shown. The tendency of the catalysts to form carbon deposits during glycerol steam reforming was calculated as the ratio between the amount of carbon obtained from TPD-TPO analysis and the amount of carbon converted during the catalytic reaction (selectivity to carbon deposit S_C in mmol C_{total} $molC^{-1}_{converted}$).
- The re-oxidation capacity of the catalysts (50 mg) was estimated after a reduction for 1 h at 700 °C (15 °C min^{-1} under 1% H_2/He mixture). This procedure was referenced as $H_{2(TPR)}$. The reduced catalyst was cooled to room temperature under helium and the re-oxidation experiment was started. The sample was heated again at 15 °C min^{-1} to 700 °C under 50 ml min^{-1} of 1% O_2/He mixture. The quantity of oxygen consumed by the reduced solid upon heating was defined as $O_{2(TPO)}$. These measurements were carried out in PFEIFFER vacuum spectrometer following the *m*/*z* signals 2, 16, 18, 28, 32 and 44. Only the results of *m*/*z* signals 2 (H_2) and 32 (O_2) are shown.
- The re-oxidation and re-reduction capacity were also studied using H_2 and O_2 pulses until no further H_2/O_2 consumption. In both cases, pulses of 500 μl of H_2/O_2 were injected on the catalyst at 650 °C. First, 20 mg of the fresh catalysts were reduced by pulses of 10% H_2/Ar. The catalysts were then re-oxidized with 10% O_2/He pulses. Finally, the catalysts were reduced again by H_2-rich pulses. The following procedure was applied: 30 pulses of 10% H_2/Ar for the first reduction; 10 pulses of 10% O_2/He pulses for the re-oxidation; and 40 pulses of 10% H_2/Ar for the re-reduction. The experiments were performed in a Micromeritics AutoChem II 2920 equipment using a TCD detector.

3. Results and discussion

3.1. Characterization of fresh catalysts

A complete characterization of similar catalysts has already been published elsewhere [5,27]. However, for the purpose of this study, we include some of the more relevant conclusions and discussion of the characterization results, emphasizing the effect of the ceria amount on the physico-chemical properties of the catalysts.

As a general conclusion of the XRD study (Fig. 1A), it is established that the pseudo-sol–gel method allows the formation of fluorite type mixed oxide structure. However, for the three catalysts, a small segregation of Co_3O_4 (Co_3O_4 peaks at 36.8° and 65.2° - JCPDS 43-1003) is also observed. Peaks related to Rh_2O_3 (JCPDS 24-0924) are not noticed, probably due to the low quantity of Rh in the catalysts, below the detection limit of the XRD technique. For CZ^ICoRh, peaks at $2\theta = 29.1°$, 33.7°, 48.5°, 57.5°, 60.4°, 71.5° and 78.5°, which corresponds to the cubic fluorite structure $Ce_{0.6}Zr_{0.4}O_2$ (JCPDS 38-1439), are observed. These peaks are shifted to higher and lower 2θ for CZ^PCoRh and CZ^RCoRh, respectively. For CZ^PCoRh, peaks of fluorite structure $Ce_{0.16}Zr_{0.84}O_2$ (JCPDS 38-1437) are observed, while peaks of $Ce_{0.75}Zr_{0.25}O_2$ (JCPDS 28-0271) are observed for CZ^RCoRh.

The increase of the cerium content increases the cubic lattice parameter "*a*" (Table 1). For CZ^PCoRh the value of "*a*" corresponds to 5.18 Å, while it increases until 5.29 and 5.34 Å for CZ^ICoRh and CZ^RCoRh respectively. The cubic lattice parameter has been reported as 5.41 Å for CeO_2 [29,30] and 5.29 Å for $Ce_2Zr_2O_8$ [26]. The insertion of Zr^{4+} into the fluorite structure decreases the cell

Table 1
Cubic lattice parameters "*a*", average crystallite of CZ and Co size and textural properties for fresh catalysts.

Catalysts	Lattice "*a*" (Å)	Average crystallite size of CZ (nm)	Average crystallite size of Co_3O_4 (nm)	BET Surface ($m^2\ g^{-1}$)	Pore volume ($cm^3\ g^{-1}$)
CZ^PCoRh	5.18	7.3	14.1	20	0.052
CZ^ICoRh	5.29	5.4	19.6	21	0.054
CZ^RCoRh	5.34	6.1	17.1	40	0.088

volume because of the lower ionic radii of Zr^{4+} (0.84 Å) with respect to the ionic radii of Ce^{4+} (0.97 Å) [31]. The increase of zirconium amount induces the cell shrinkage and decreases the lattice parameter [32]. The decrease of the cubic lattice parameter observed for CZ^PCoRh could also be related to a better insertion of cobalt into the fluorite structure. As has been proven elsewhere [28], Co^{2+} cations can partially substitute Zr^{4+} cations in the CZ lattice. The smaller ionic radius of Co^{2+} (0.73 Å), and the higher amount of zirconium in CZ^PCoRh would promote the insertion of cobalt into the lattice, decreasing the value of "*a*". Table 1 also presents the CZ and Co_3O_4 crystallite sizes calculated from XRD patterns using the Scherrer equation. The smallest size of Co_3O_4 crystallites is observed for CZ^PCoRh (14.1 nm). This characteristic is in agreement with a better insertion of cobalt into the fluorite structure, promoted by the higher amount of zirconium.

The crystalline structure of CZCoRh catalysts has been also characterized by Raman spectroscopy (Fig. 1B). For comparison purposes the Raman spectra of CeO_2, Co_3O_4, $Ce_2Zr_2O_8$ (CZ^I) and $Ce_2Zr_{1.5}Co_{0.5}O_{8-\delta}$ (CZ^ICo) are also included. Pure CeO_2 shows two main bands: the most intense at 462 cm^{-1} is ascribed to the Raman active F2g mode and it corresponds to the oxygen symmetric vibration around Ce^{4+} [33]. The very weak band at 598 cm^{-1} is assigned to the presence of oxygen vacancies in the structure [34] and it indicates the Ce^{3+} ions existence. The CZ^I support exhibits another two additional Raman-active modes at 185 and 303 cm^{-1} typical of $Ce_2Zr_2O_8$ structure. The appearance of these bands is attributed to the displacement of the O atoms from their ideal fluorite lattice position by zirconium insertion [35,36]. The typical bands at 462 and 598 cm^{-1} for CeO_2 appear to shift to the right until 470 and 629 cm^{-1} respectively as a consequence of the lattice contraction brought about by zirconium ion insertion in CZ support.

The typical Raman spectra are totally different for Co containing catalysts. The cobalt in the CZ lattice deforms the structure. The intensity of the characteristic peaks of the fluorite structure changes and the Co_3O_4 peaks are superimposed over fluorite peaks as has been pointed out elsewhere [27,37]. The deformation of CZ structure has been reported to favor oxygen mobility, changing the *redox* behavior of the material and improving the Ce^{4+} reduction [37]. The peaks of Co_3O_4 are shifted with respect to the characteristic peaks of Co_3O_4 nano-crystals (191, 470, 512, 606 and 671 cm^{-1} [38]), suggesting differences in the structure or/and particle size of the cobalt oxide, probably related with the amount of ceria.

The structural changes with the increase of the ceria amount under reductive and oxidative atmospheres were studied by *in situ* Raman spectroscopy for CZ^RCoRh (Fig. 2). These results were compared with those previously obtained for CZ^ICoRh [27]. We found that the degree of Co insertion depended on the amount of ceria and its behavior changed with the atmosphere used (reductive or oxidative). For CZ^ICoRh, the Co_3O_4 spinel was always observed in reductive conditions until 150 °C. Beyond this temperature the spinel phase disappeared and the peaks corresponding to the CZ support were observed. Under oxidative conditions the spinel Co_3O_4 was not recovered. It was suggested [27] that rhodium would stabilize the cobalt inserted into the fluorite structure or at least it would inhibit the cobalt rejection after reduction at 450 °C (temperature used in the reduction protocol).

For CZ^RCoRh (Fig. 2) the Co_3O_4 spinel behavior in reductive conditions was similar to that obtained for CZ^ICoRh. The Co_3O_4 spinel almost disappeared with the increase of temperature and with the presence of H_2. However, contrary to CZ^ICoRh, after passing synthetic air, the Co_3O_4 spinel was recovered for CZ^RCoRh (Fig. 2B). In this case, the Co_3O_4 spinel peaks were shifted with respect to the peaks obtained at room temperature, as was previously observed in Fig. 1B. According to these results, the Co_3O_4 rejection should be also related to the amount of zirconium in the catalysts and not only to the stabilization of Co into the structure by the Rh presence, since Co^{2+} is normally inserted in the fluorite structure in exchange of Zr^{4+} ions [26]. The low content of zirconium for CZ^RCoRh would disfavor the cobalt insertion, promoting the Co_3O_4 rejection from the mixed oxide more than the catalyst with intermediate amount of zirconium CZ^ICoRh.

In order to prove that the homogeneity of the catalysts is related to the low ceria content (or high amount of zirconia) TEM/EDX analyses were performed (Fig. 3). From the figures, CZ particle size can be estimated between 5 and 10 nm. These values

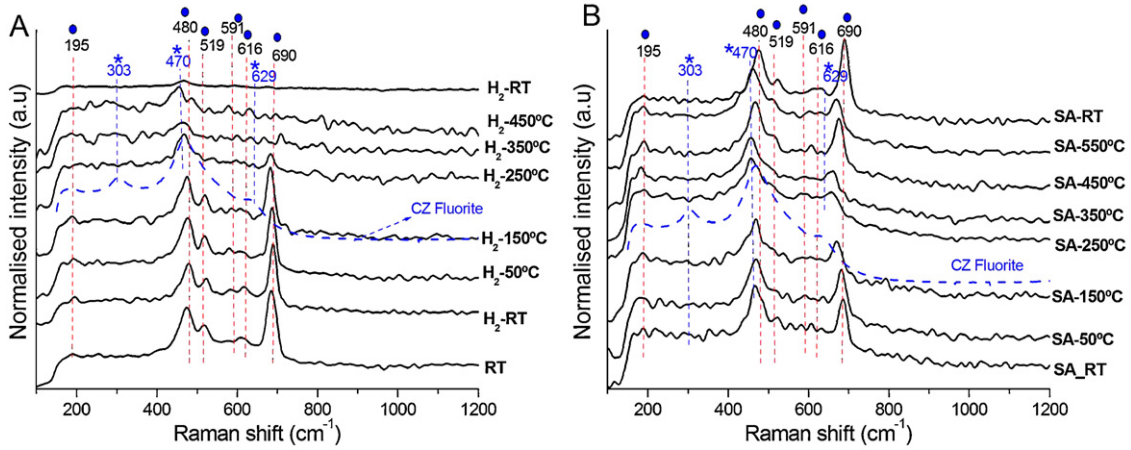

Fig. 2. Raman *in situ* of CZ^RCoRh during reduction and oxidation procedures. Symbols: (*) CZ oxide and (●) Co_3O_4 spinel.

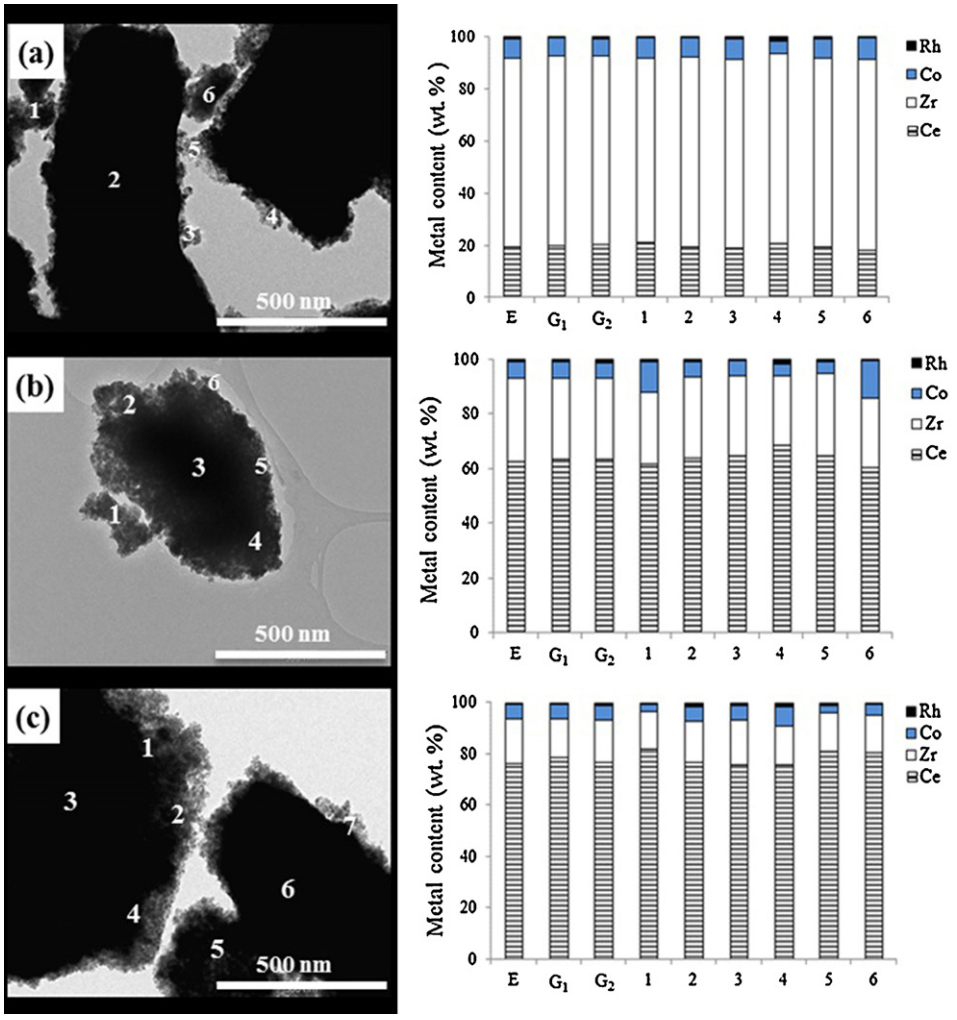

Fig. 3. Micrographs and EDX microanalyses of: (a) $CZ^{P}CoRh$, (b) $CZ^{I}CoRh$, (c) $CZ^{R}CoRh$. (G) global analysis, (1–6) points of local analyses, (E) theoretical expected composition.

agree with the particle size calculated from XRD (Fig. 1A). Metallic particles of Co and Rh and single oxide patterns of Co_3O_4 or Rh_2O_3 were not observed. High homogeneity is observed for $CZ^{P}CoRh$ (Fig. 3a), where the global (G) and the local compositions are similar to the experimental expected composition (E). Therefore a better formation of the mixed oxide will be obtained, resulting in a high micro homogeneity. For $CZ^{I}CoRh$, the global composition also corresponds to the experimental expected value. However, small variations are observed at local level (Fig. 3b, local analysis: points 1 and 6), suggesting a degree of heterogeneity among the catalyst crystallites. For $CZ^{R}CoRh$ (Fig. 3c), the global composition is slightly different from the experimental expected value varying from one global measure to the other. For the local analyses, the differences with the expected composition are more noticeable (Fig. 3c) indicating an important degree of heterogeneity. The low amount of Zr^{4+} in $CZ^{R}CoRh$ would disfavor the insertion of Co^{2+} into the lattice decreasing the homogeneity of the catalyst, confirming the results previously pointed out by XRD and Raman *in situ*.

The textural properties of the fresh catalysts are also shown in Table 1. The increase in the ceria amount increases the catalytic surface area until 40 $m^2\ g^{-1}$ with respect to ≈20 $m^2\ g^{-1}$ for $CZ^{P}CoRh$ and $CZ^{I}CoRh$. This enhancement is in agreement with the higher pore volume observed for $CZ^{R}CoRh$ compared to the pore volume determined for $CZ^{P}CoRh$ and $CZ^{I}CoRh$.

The effect of Co and Rh insertion on the reducibility of CZ mixed oxide catalyst has been extensively studied elsewhere [5,25,27]. However, the effect of the ceria amount on reducibility properties has not yet been discussed. For this purpose, three different characterization protocols were used: H_2-TPR to examine the total reducibility of the catalyst; oxidation after reduction conditions to determine the re-oxidation capacity ($H_{2(TPR)}$ and $O_{2(TPO)}$); and reduction/oxidation/reduction with pulses at the reaction temperature to evaluate the re-reduction capacity of the catalysts.

It is known that CZ fluorite type oxide catalysts have two reduction temperatures clearly identified, one close to 620 °C that corresponds to the reduction of Ce^{4+} to Ce^{3+} at the surface, and another at 900 °C associated to the reduction of bulk Ce^{4+} [27,39,40]. Co and Rh insertion to the CZ structure significantly modifies this profile [25,27]. The presence of cobalt promotes the reduction of surface and bulk Ce^{4+} at lower temperature [27], thus favoring the mobility of oxygen in the bulk [41]. Rhodium lowers even more this temperature of reduction [25,27], providing the hydrogen necessary to reduce the bulk Ce^{4+} at much lower temperature than Co. However, it was also pointed out that for $CZ^{I}Co$ and $CZ^{I}Rh$ monometallic catalysts, the percentage of reduced cerium was similar to percentage observed for the bare CZ^{I} support (45%) [27]. Conversely, for the bimetallic $CZ^{I}CoRh$ catalyst, it was observed that the presence of both Co and Rh favored the reduction of CZ mixed oxide, decreasing the typical temperature of reduction observed for the bare CZ [42,43], but also considerably increasing the percentage of reduced cerium (88%). Therefore, it was suggested a cooperative effect between Rh and Co [27].

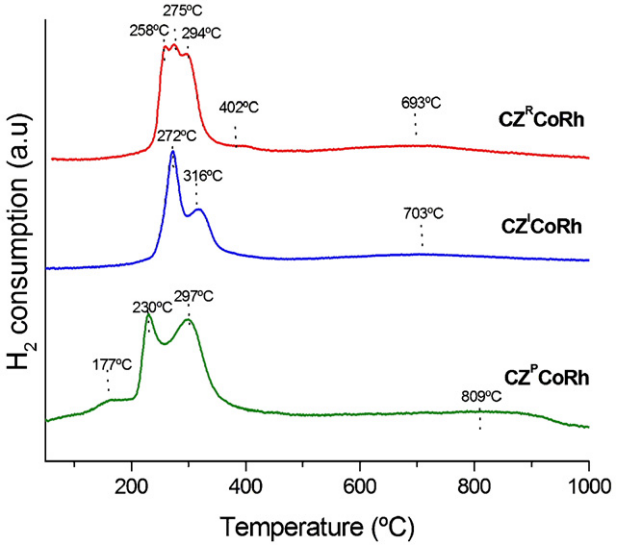

Fig. 4. H_2-TPR profiles for fresh catalysts.

The variation in the ceria amount also modifies the reducibility profile of CZ (Fig. 4). At high temperature the increase of the ceria amount decreases the temperature of the reduction peak agrees with the increase in the ceria amount from 900 °C for CZ, to 809 °C for CZ^PCoRh, to 703 °C for CZ^ICoRh and to 693 °C for CZ^RCoRh. At low temperature, the increase of the amount of cerium leads to an overlapping of the two main reduction peaks, along with a decreasing intensity. According to the previous characterization results (Figs. 1 and 2) the rejection of Co_3O_4 would be favored with the increase in the amount of ceria. The Co_3O_4 could have an important role in the reducibility behavior of the catalysts since differences in the reduction profiles at low temperature are observed for the catalysts of the current study (Fig. 4). In fact, CZ^RCoRh shows an additional small reduction peak at 402 °C, probably related to the higher amount of Co_3O_4 spinel. This result agrees with the reduction of the metallic particles of different sizes and/or with different grades of interaction with the support affecting the reducibility behavior of CZ [27,28].

Table 2
H_2-TPR results: hydrogen consumption and $\%Ce^{4+}$ reduced.

Catalysts	H_2 consumption (mmol H_2 $g^{-1}_{catal.}$)			
	Total	Low temperature	High temperature	$\%\ Ce^{4+}$ reduced
CZ^PCoRh	1.93	1.27 (66%)	0.66 (34%)	100
CZ^ICoRh	2.72	1.20 (44%)	1.52 (56%)	88
CZ^RCoRh	2.62	1.71 (65%)	0.91 (35%)	70

From TPR results, the H_2 consumption was determined for the three catalysts (Table 2). For CZ^ICoRh and CZ^RCoRh the total H_2 consumption is similar, while it is considerably lower for CZ^PCoRh. At low temperature, the highest consumption is observed for CZ^RCoRh while for CZ^PCoRh and CZ^ICoRh the consumptions are alike. Conversely, at high temperature the highest consumption is observed for CZ^ICoRh followed by CZ^RCoRh and then CZ^PCoRh. For CZ^RCoRh, the higher H_2 consumption at low temperature is favored by its higher surface area but also by the probably lower insertion of Co in the CZ lattice, according to the TEM/EDXS and Raman *in situ* results. For CZ^ICoRh, the higher H_2 consumption at high temperature could be not only related to the decrease in the surface area, but also to the higher insertion of Co in the CZ lattice making more difficult its reduction at low temperature. For CZ^PCoRh, the surface area is approximately the same as that of CZ^ICoRh. This agrees with the similar values of H_2 consumed at low temperature. The lower H_2

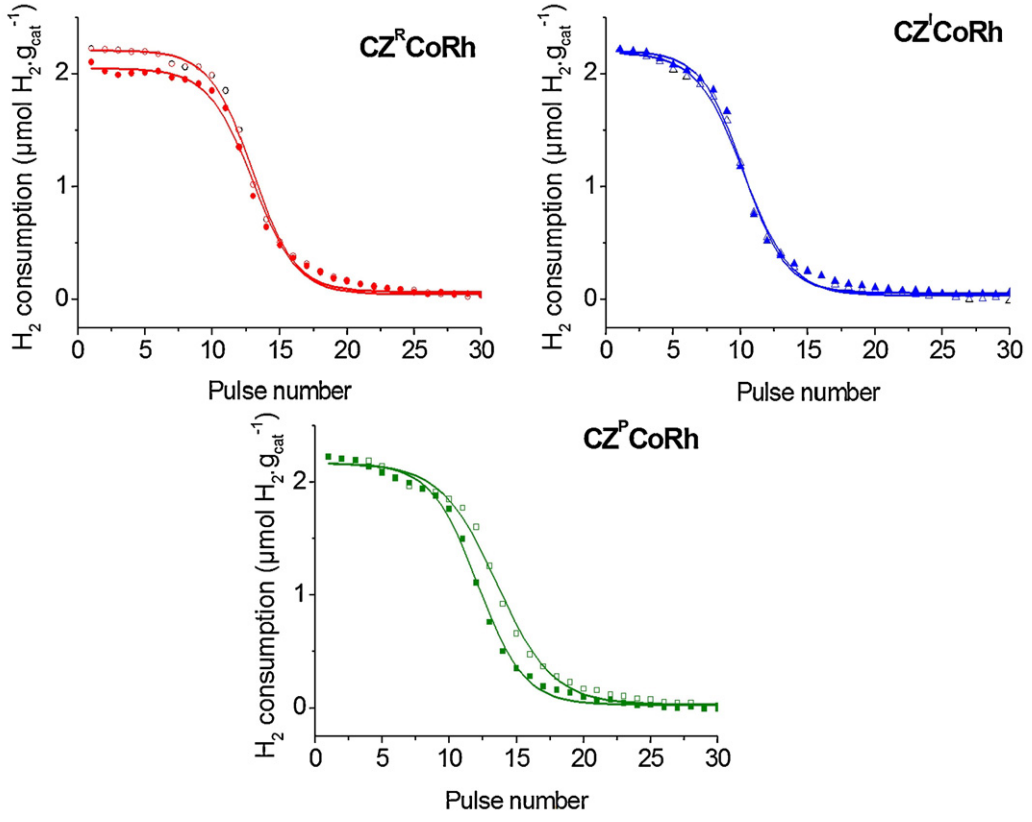

Fig. 5. H_2 pulses for first reduction (open symbols) and for second reduction after oxidation (filled symbols) for fresh catalysts.

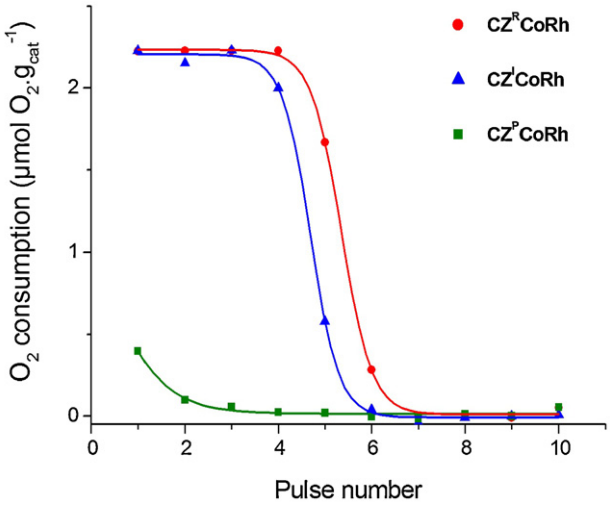

Fig. 6. O_2 pulses after a first reduction for fresh catalysts.

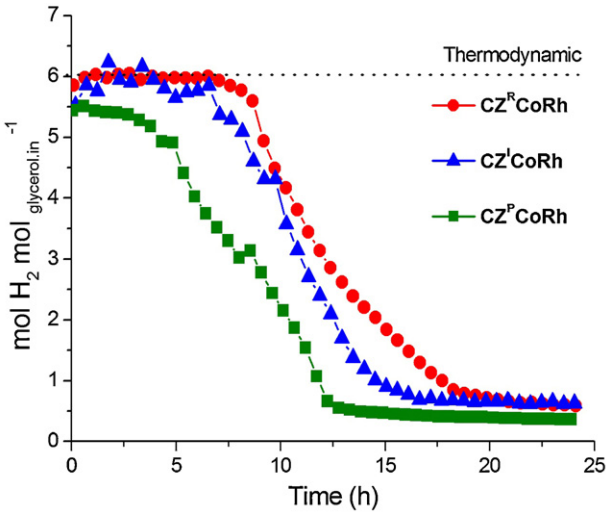

Fig. 7. Evolution of the H_2 production in glycerol steam reforming. Conditions: temperature 650 °C, H_2O:glycerol molar ratio 9:1 and atmospheric pressure. Thermodynamic value expected using the UNIQUAC model: 6.06 mol H_2 $mol^{-1}_{glycerol.in}$.

consumption at high temperature is simply explained by the lower content of Ce^{4+} in the bulk for CZ^PCoRh compared to CZ^ICoRh.

The percentage of reduced cerium follows the next decreasing order: $CZ^PCoRh > CZ^ICoRh > CZ^RCoRh$ (Table 2). This decrease with the increase in the cerium content can be related to the enhancement of the oxygen mobility with the increase in the content of zirconium observed in CZ catalysts [44]. The activation energy of oxygen migration was found to decrease with increasing the zirconium content [45].

Fig. 5 shows the results of H_2 consumption by pulse number during the first reduction and the second reduction in a reduction/oxidation/reduction experiment. For CZ^PCoRh the H_2 consumption is similar for both reduction stages during the first pulses. However after 9 pulses the H_2 consumption is lower in the second reduction than in the first reduction. Thus, the second reduction is more difficult when part of cerium is already reduced. For CZ^ICoRh, the same profile is noticed during both reduction stages. This catalyst shows the best *redox* behavior. On the other hand, for CZ^RCoRh, the H_2 consumption is lower in the second reduction than in the first reduction. At the beginning of the second reduction, CZ^RCoRh is not able to uptake the whole incoming H_2, decreasing the capability of oxygen migration with respect to the first reduction procedure.

Fig. 6 presents the evolution of O_2 consumption by pulse number after the first reduction. It is observed that the re-oxidation of the mixed oxide catalysts is high at high ceria content for CZ^RCoRh and CZ^ICoRh. At low ceria content (CZ^PCoRh) the O_2 consumption is significantly lower compared to the others, in agreement with the lower re-oxidation capacity shown in results of Table 3.

The improved re-oxidation capacity with the increase of the ceria amount is also confirmed by the O_2 consumption ($O_{2(TPO)}$) and the H_2 consumption ($H_{2(TPR)}$) during the experiments of re-oxidation capability at 700 °C (Table 3). Simultaneously with the increase in the ceria amount, the amount of O_2 uptake increases along with the amount of H_2 consumption for all catalysts. This characteristic indicates the effective re-oxidation capacity of the samples which was also verified by the $O_{2(TPO)}/H_{2(TPR)}$ ratio. For all catalysts, the $O_{2(TPO)}/H_{2(TPR)}$ ratio is close to 0.5, which is the amount of oxygen atoms required to eliminate one atom of hydrogen. The increase in ceria favors the amount of O_2 uptake. This is higher for CZ^ICoRh and CZ^RCoRh than the corresponding value for the mixed oxide re-oxidation ($O_{2(TPO)}/H_{2(TPR)} > 0.5$), while it is lower for CZ^PCoRh ($O_{2(TPO)}/H_{2(TPR)} = 0.48$). For CZ^ICoRh, the higher $O_{2(TPO)}/H_{2(TPR)}$ ratio agrees with the maximal H_2 consumption observed by H_2-TPR at high temperature.

The analysis of the *redox* properties of the catalysts with different amounts of ceria points out two different aspects: the global capacity of H_2 consumption and the capacity to be re-oxidized and re-reduced. The total amount of H_2 consumed was logically higher for CZ^RCoRh and CZ^ICoRh, due to the higher amount of Ce^{4+} that is able to be reduced in the materials. However, these catalysts also showed a significantly higher re-oxidation capacity compared to CZ^PCoRh. The best *redox* behavior (reduction–oxidation–reduction capacity) was observed for CZ^ICoRh. This catalyst shows a higher ability to store and to release oxygen, probably due to the beneficial properties induced by an intermediate content of zirconium and the intermediate content of ceria. The bulk of CeO_2 behaves as an oxygen reservoir, supplying oxygen to the surface through a migration process; while under less reductive environment, the opposite process is likely, and the lattice oxygen is replenished by oxygen coming from the gas phase [46,47]. The introduction of zirconium, in a certain extent, creates a distortion of the lattice that increases the oxygen mobility in the bulk oxide [48–50].

3.2. Activity results

Fig. 7 shows the evolution of H_2 production for 24 h of glycerol steam reforming at 650 °C. The H_2 production is expressed as mol of H_2 produced per mole of glycerol introduced. For the three catalysts the hydrogen production at the beginning of the reaction was higher than 5.5 mol H_2 $mol^{-1}_{glycerol.in}$. For CZ^ICoRh and CZ^RCoRh, the thermodynamic expected value under our reaction conditions was obtained for several hours. The time at high production of H_2 is longer at high ceria content in the catalyst. H_2 production around 6.0 mol H_2 $mol^{-1}_{glycerol.in}$ is maintained for 3, 7 and 9 h for CZ^PCoRh, CZ^ICoRh and CZ^RCoRh, respectively. Then, the H_2 production progressively decreases with time, reaching 0.5 mol H_2 $mol^{-1}_{glycerol.in}$ after 19 h, 16 h and 12 h of reaction for CZ^RCoRh, CZ^ICoRh and CZ^PCoRh, respectively.

Fig. 8 shows the evolution with time on stream of the weighted mean conversions (X, X_G and X_L) for glycerol steam reforming. All the results are presented for the three intervals of time of liquid fraction recovery (0–5 h, 5–8.5 h and 8.5–24 h). Glycerol can be effectively transformed by all the catalysts during the first 8.5 h of reaction ($X \approx 100\%$). However, the ability to convert glycerol is progressively lost. After 8.5 h, X decreases to 67% for CZ^PCoRh, 64% for CZ^ICoRh and 77% for CZ^RCoRh. The decrease

Table 3
H_2 consumption and O_2 uptake obtained after TPR-TPO.

Catalysts	H_2 consumption μmol H_2 $g^{-1}_{catal.}$ (from $H_{2(TPR)}$)	O_2 storage μmol O_2 $g^{-1}_{catal.}$ (from $O_{2(TPO)}$)	$O_{2(TPO)}/H_{2(TPR)}$)
CZ^PCoRh	1777	854	0.48
CZ^ICoRh	2220	1172	0.53
CZ^RCoRh	2404	1244	0.52

of X_G, which follows the same tendency of X, is more pronounced. Both X and X_G are improved by the increase of the ceria amount ($CZ^RCoRh > CZ^ICoRh > CZ^PCoRh$), while X_L decreases in the opposite order ($CZ^RCoRh \approx CZ^ICoRh < CZ^PCoRh$). In all cases, the conversion to non-condensable products is favored with respect to the conversion to condensable products ($X_G \gg X_L$) but this difference decreases with time on stream. The three catalysts progressively lose selectivity to products in the gas phase under reaction conditions, along with the loss of activity in glycerol conversion.

The activity results correspond to 86% of hydrogen yield, at 100% of conversion, and around 10%, when the conversion to non-condensable products (X_G) decreases until 22%. These values are comparable to the results recently reported by Gallo et al. [51], where the H_2 yield remained at 81% for several hours using Ru based catalysts at 650 °C. The higher catalytic stability presented by the latter could be related to the higher amount of noble metal per mole of fed glycerol (5.2 mol_{Ru} s $mol^{-1}_{glycerol}$), compared to the amount of rhodium used for the present study (2.4 mol_{Rh} s $mol^{-1}_{glycerol}$). On the other hand, the presence of cobalt would also account as active phase, increasing the space velocity to 40.5 mol_{Rh+Co} s $mol^{-1}_{glycerol}$. However, for catalysts based on transition metals, the space velocity is considerable higher compared to noble metal-based catalysts (306 mol_{Ni} s $mol^{-1}_{glycerol}$) [17]. The performances observed for CZCoRh catalysts are considerable higher for similar conditions: 72% of conversion and approximately 65% of H_2 yield (650 °C) [17].

Fig. 9 shows the effect of the ceria amount on the distribution of non-condensable products (H_2, CO_2, CO, CH_4 and C_2H_4) expressed as mole of product per mole of glycerol converted into gaseous products. In all cases, two different reaction zones can be observed: *Zone A*, at high H_2 concentrations close to 6 mol H_2 $mol^{-1}_{glycerol.Conv.gas}$; and *Zone B*, at low H_2 concentrations close to 3 mol H_2 $mol^{-1}_{glycerol.Conv.gas}$. In *Zone A*, the production of H_2 and CO_2 is favored; while in *Zone B* the formation of CO, C_2H_4 and CH_4 is favored. CZ^RCoRh is the most stable catalyst in *Zone A*, with high H_2 production for a longer time (for 9 h of reaction) while it was only 7 h and 1 h for CZ^ICoRh and CZ^PCoRh, respectively. After this time, the deactivation is clear (*Zone B*). This last stage appears after 11 h of reaction for CZ^PCoRh, 13 h for CZ^ICoRh and 17 h for CZ^RCoRh. For the three catalysts, C_2H_4 appears just after H_2 concentration starts to decrease.

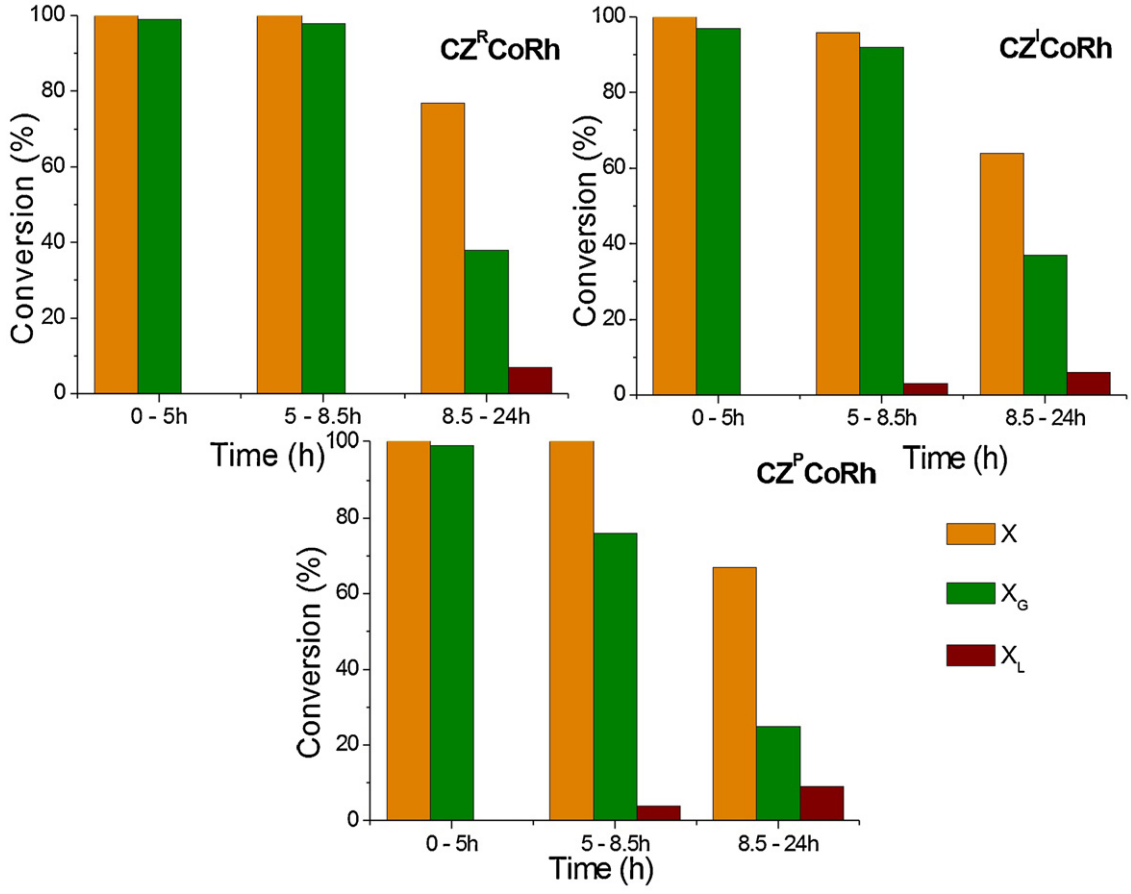

Fig. 8. Evolution with time of reaction of weighted mean conversions for glycerol steam reforming. X (global conversion), X_G (conversion to non-condensable products) and X_L (conversion to condensable products).

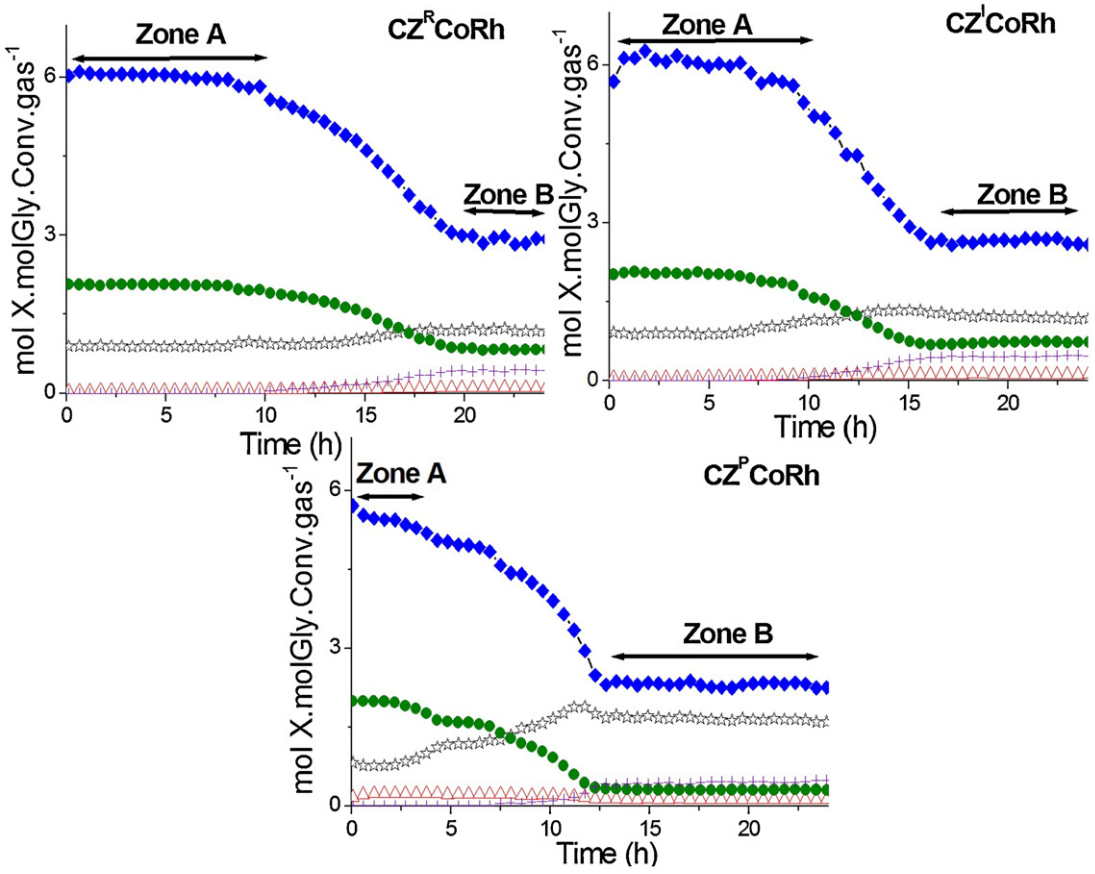

Fig. 9. Distribution of non-condensable products in glycerol steam reforming. ♦ H_2, ☆ CO, △ CH_4, ● CO_2, + C_2H_4.

For CZ^PCoRh, the CH_4 production is always slightly higher, which is in agreement with the lower production of H_2, compared to CZ^ICoRh and CZ^RCoRh. This is consistent with the lower re-oxidation capacity of this catalyst discussed above (Fig. 6), probably favoring the hydrogenation of carbon with respect to its oxidation.

For all catalysts the formation of condensable products is not observed in the first 5 h of reaction (Fig. 8). After this time, the formation of small quantities of hydroxyacetone was detected for CZ^PCoRh and CZ^ICoRh, along with traces of acetaldehyde and acrolein in the case of CZ^PCoRh. For CZ^RCoRh, the formation of condensable products starts only after 8.5 h of reaction. The distribution (molar fraction) of condensable products between 8.5 and 24 h of reaction is presented in Fig. 10. The main product is always hydroxyacetone. It is followed by the production of acetaldehyde and acrolein and traces of methanol > ethylene glycol > propylene glycol > acetic acid. The lower formation of condensable products for the catalyst rich in ceria is in agreement with the highest X_G observed over the whole reaction. Thus, it can be said that the increase of ceria amount delays the production of the condensable products, favoring the selectivity into non-condensable products (H_2, CO_2, CO, CH_4 and C_2H_4).

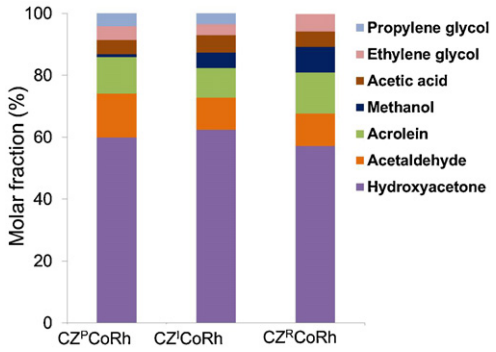

Fig. 10. Molar distribution within the condensable products in glycerol steam reforming over the period of time 8.5–24 h.

In a previous work [27], we pointed out that in glycerol steam reforming at 650 °C two effects coexisted: the catalytic effect that favors the H_2 and CO_2 production, and the thermal effect that enhanced the glycerol decomposition. This strong thermal effect at temperatures higher than 600 °C was also pointed out for others authors, in catalytic cracking of glycerol [52] and in catalytic glycerol steam reforming [53,54]. Therefore, the catalytic activity was related to the capacity of the catalyst to further activate and transform H_2O during the steam reforming reaction. When the deactivation is strong, the catalyst is less capable to activate H_2O either to reform glycerol or to reform the by-products toward H_2. Thus, the steam reforming is blocked and the glycerol decomposition is predominant [27].

In order to establish the effective participation of H_2O in the glycerol steam reforming reaction, the H-atoms balance was calculated for the non-condensable products (H_2, CO_2, CO, CH_4 and C_2H_4) (Fig. 13). For a complete glycerol steam reforming the balance of H-atoms will be 8H-atoms coming from the glycerol molecule ($C_3H_8O_3$) and 6H-atoms coming from 3 molecules of water, in total 14H-atoms. For glycerol decomposition only 8H-atoms from glycerol appears. For the CZ^ICoRh and CZ^RCoRh the balance of H-atoms was higher than 12H-atoms per mol glycerol converted in gas phase at the beginning of the reaction. This indicates that H_2O is largely involved in the formation of non-condensable products. For

Table 4
Quantification of the carbonaceous deposits after glycerol steam reforming.

Catalysts	mmol $C_{total}\ g^{-1}_{catal.}$	S_C mmol $C_{total}\ molC^{-1}_{converted}$
CZ^PCoRh	2.51	0.17
CZ^ICoRh	1.50	0.10
CZ^RCoRh	1.19	0.07

CZ^PCoRh the H-atoms balance in gas phase was 12 at the beginning suggesting the lower participation of H_2O with respect to the others. That balance decreased progressively with the time of reaction reaching approximately 8-atoms per mol of glycerol converted into gas phase products in Zone B of activity. So, during the last period of time the catalyst would progressively lose its ability to activate H_2O and the H-atoms balance will approach the balance observed for glycerol decomposition as was pointed out elsewhere [27].

According to the different observations during the reaction and the discussion above, the capacity to active H_2O under the reaction conditions is improved by the increase of the ceria amount. The catalyst rich in ceria favors for a longer time the steam reforming until H_2 and CO_2 than the others. The improved selectivity with this catalyst could be ascribed to the improvement of different physico-chemical properties inherent to higher ceria amount such as: surface area, reducibility and re-oxidation capability.

3.3. Characterization of spent catalysts

One of the possible causes of deactivation of Co-based catalysts in steam reforming reactions is the oxidation of the metallic phase (Co^0). However, for the CoRh-based mixed oxide catalysts studied here, would not be a notorious inconvenience since a cooperative effect between Co and Rh in steam reforming reactions was already observed [27,55,56]. The presence of Rh would inhibit the oxidation of cobalt under reaction conditions by promoting the reducibility of Co. That positive effect was also confirmed in TPR results.

In order to determine other possible causes of the catalyst deactivation XRD, HRTEM and TPD-TPO characterizations were performed after glycerol steam reforming.

For all the samples after test, intense peaks at $2\theta = 35.6^\circ$, 41.4°, 60.0° and 71.6° were observed by XRD (results not shown). These peaks correspond to the silicon carbide (JCPDS 03-065-0360), used as diluent for the reaction, which considerable attenuated the signal initially observed (Fig. 1a). In spite of this interference, the characteristic peaks of the fluorite structure were also noticed for the three catalysts, indicating the preservation of the fluorite structure after 24 h of reaction.

The peak at 36.8° ascribed to the Co_3O_4 spinel phase was no longer observed, may be only hindered by the intense peak of SiC at 35.6°.

The formation of carbon deposits was studied by TPO experiments (Fig. 11). For all spent catalysts a peak of high intensity at 700 °C and another less intense at 362 °C are observed. In addition, peaks of CO_2 at 531 °C and 488 °C are noticed for CZ^PCoRh and CZ^ICoRh, respectively. Table 4 shows the quantification of the carbonaceous deposits and the selectivity toward the formation of carbon deposits (S_C). The carbon formation decreases when the ceria amount increases. After reaction, 2.51, 1.50 and 1.19 mmol $C_{total}\ g^{-1}_{catal.}$ are formed on CZ^PCoRh, CZ^ICoRh and CZ^RCoRh, respectively. Those values correspond to Sc of 0.17, 0.10 and 0.07 mmol $C_{total}\ molC^{-1}_{converted}$, respectively. For the catalyst with low ceria content, the high quantity of carbon deposits and the high value of S_C can be related to the low re-oxidation capacity of the material.

According to HRTEM results, two kinds of carbon formation are effectively observed after reaction: surface carbon and filamentous carbon (Fig. 11 - representative micrographs for spent CZ^ICoRh catalyst). It is known that surface carbon can be oxidized at low temperature and the filamentous carbon at high temperature during TPO experiments [57,58]. The three catalysts show a similar oxidation peak at high temperatures in TPO (Fig. 11). The formation of filamentous of carbon is favored compared to the formation of surface carbon. For CZ^PCoRh a non-negligible oxidation at low temperature is observed. The accumulation of surface carbon for this catalyst is once again in agreement with its low re-oxidation capability. In summary, low amount of ceria in CZ^PCoRh leads to a low re-oxidation capability of the material. As a consequence, carbon species at the surface of the metallic particles are either hydrogenated into CH_4 or simply accumulate on the surface, decreasing rapidly the activity of the catalyst.

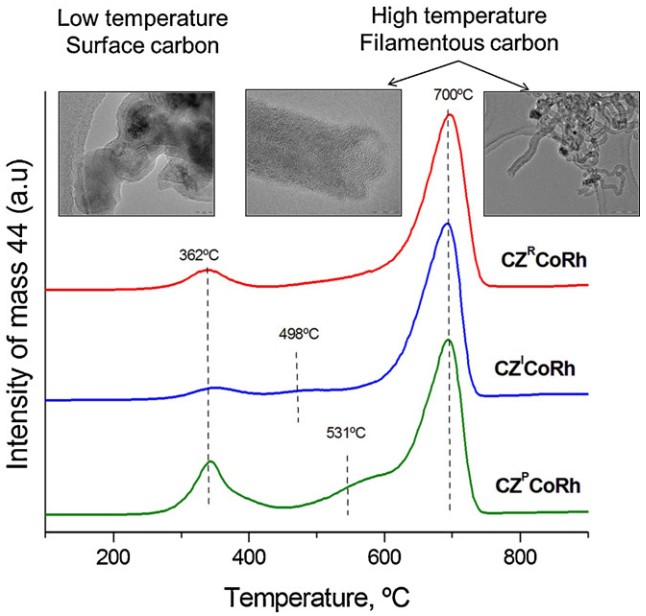

Fig. 11. TPO profiles for spent catalysts and representative HRTEM micrographs for spent CZ^ICoRh catalyst.

The characterization of the catalysts after test shows that at the actual reaction conditions the formation of carbon deposits could be the main deactivation cause. The carbon deposition is widely recognized as one of the main deactivation causes in steam reforming of light hydrocarbons [59,60]. In glycerol steam reforming, recent works have also related the loss of catalytic activity to the formation of superficial carbon and coke [54,61]. This kind of deactivation has been related to the blocking of the active size, either by direct carbon deposition or by blocking the access to the active site (pores) [53], or by the formation of encapsulating coke that quickly deactivates the particles [61,62].

On the other hand, the formation of carbon deposits could also be a consequence of the active metal sintering [58], which would lead to the catalyst deactivation by the formation of carbon deposits but also by the decreasing of the catalytic active surface. Chiodo et al. [54], studied this hypothesis using Rh- and Ni-based catalysts at different reaction temperatures (923–1073 K). However, by TEM investigations, they concluded that the increase in the particle size was not enough to justify the deactivation observed.

In order to confirm if the deactivation of the catalyst was mostly related to the formation of carbon deposits, three consecutive tests (steam reforming/oxidation reactions) were performed using a flow of oxygen to burn the C deposits generated after the reforming reaction. After each "cleaning procedure" the catalyst was again reactivated by reduction before the following reaction cycle.

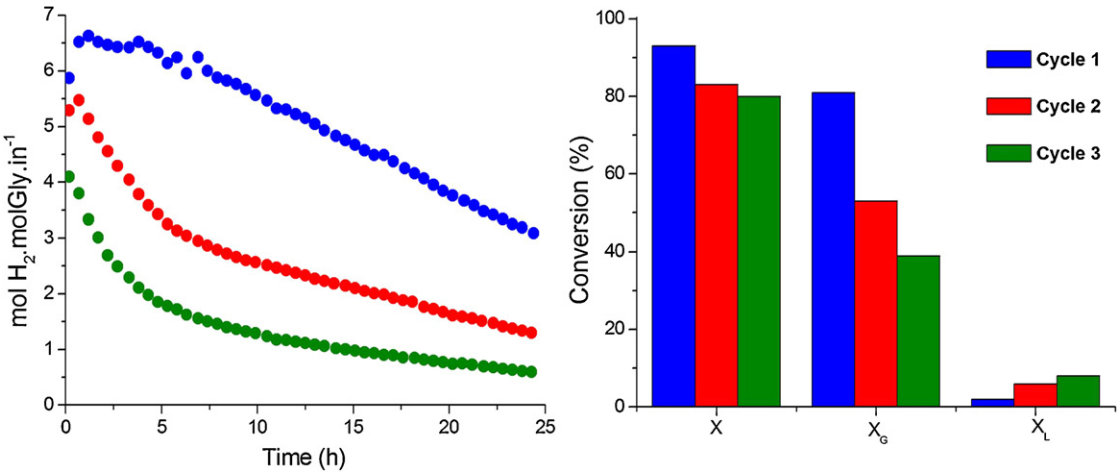

Fig. 12. Evolution of (a) H_2 production, and (b) weighted mean conversions per cycle of glycerol steam reforming after cleaning with oxygen. Conditions: temperature 650 °C, H_2O: glycerol molar ratio 9:1 and atmospheric pressure.

Fig. 12 shows the H_2 production after glycerol steam reforming/oxidation cycles for the most active catalyst CZ^RCoRh. A significant part of the initial activity was decreased after each cycle. This loss of catalytic activity was also observed in the weighted mean conversion values (Fig. 12B). The capacity to convert glycerol to non-condensable products was considerably decreased, while the conversion to condensable products increased after each cleaning and reactivation process. Therefore, the regeneration procedure by oxidation was not sufficient to recover the initial catalytic behavior of the catalyst. Assuming that a 4 h-oxidative treatment at 650 °C was enough to eliminate the carbon deposits evidenced by TPO (broad peak around 700 °C under dynamic conditions), the deactivation is clearly not only due to the formation of carbon deposits. The metal particle sintering was effectively another cause of deactivation, closely related to the formation of carbon deposits [58].

As summary, it is clear that *Zone B* of reactivity, related to the deactivation of the catalysts, appears when the catalytic behavior is affected by the carbon deposits. The catalyst loses part of the capacity to activate water. The glycerol decomposition is predominant, with low H_2 production and with high production of hydroxyacetone and acrolein. The formation of these condensable products would also favor the carbon formation [63,64], reducing even more the catalytic performance of the catalysts. From acrolein, the production of coke has been reported by further dehydration of the molecule; and from hydroxyacetone, the oligomerisation to form polyglycerol species, which may lead to carbon deposits, has been also described (Fig. 13).

The decrease of the carbon formation with the increase of the ceria amount and, consequently, the improvement of the H_2 production can be ascribed to the improved re-oxidation capacity, enhancing the gasification of the carbon deposits.

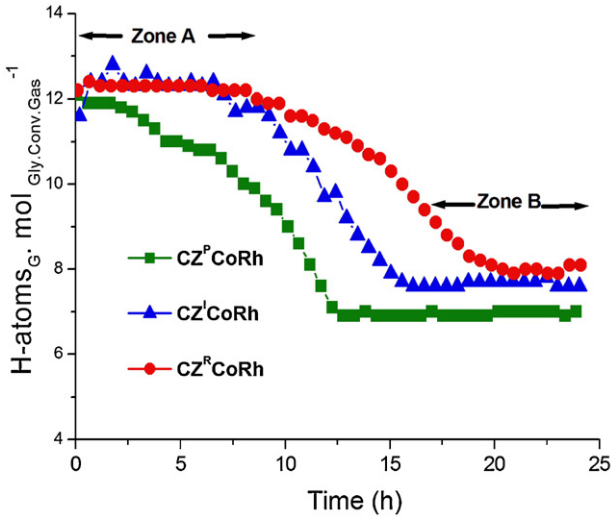

Fig. 13. Balance of H-atoms in the gaseous phase products per mol of glycerol converted in gaseous phase.

4. Conclusions

The catalytic behavior of glycerol steam reforming for H_2 production is highly affected by the Ce/Zr ratio since the stability, selectivity and activity of the catalysts are improved by an increase of the ceria content. This is the reason of the enhanced reducibility properties, higher oxidation capacity, thus improved gasification ability.

At the beginning of the steam reforming reaction all the catalysts are active and selective to H_2. The loss of the catalytic activity was observed by the decrease of the global conversion along with a change of selectivity, increasing the formation of condensable products (mainly hydroxyacetone), CO and C_2H_4, and decreasing the formation of H_2 and CO_2. The reforming capability of the catalysts decreases and the glycerol decomposition must be considered. Thus, the difference in the catalytic stability and activity of the catalysts is linked to their capability to activate the H_2O under reaction conditions to favor the steam reforming reaction over the decomposition reaction. The increase of the ceria amount favors the activation of H_2O for a longer period of time allowing the carbon gasification and delaying the deactivation of the catalyst.

Acknowledgments

Financial support by program ECOS-Nord No Co8P03 COLCIENCIAS/ICFES/ICETEX (Colombia-France) and program Picasso No. 22905RD (France-Spain) are gratefully acknowledged. L.M. Martínez T also acknowledge the Spanish "Ministerio de Ciencia e Innovación" for financial support (ref. no. 2008-0559). The authors acknowledge Dr. Miguel Ángel Centeno Gallego (Instituto de Ciencia de Materiales de Sevilla, Centro Mixto CSIC- Universidad de Sevilla - Spain) for the Raman experiments and also acknowledge Daniel Schwartz for the English revision.

References

[1] P.D. Vaidya, A.E. Rodrigues, Chemical Engineering and Technology 32 (2009) 1463–1469.
[2] T. Hirai, N.O. Ikenaga, T. Mayake, T. Suzuki, Energy and Fuels 19 (2005) 1761–1762.
[3] P. Ramírez de la Piscina, N. Homs, Chemical Society Reviews 37 (2008) 2459–2467.
[4] J. Sehested, Catalysis Today 111 (2006) 103–110.
[5] M. Araque, L.M. Martínez T, J.C. Vargas, A.C. Roger, Catalysis Today 176 (2011) 352–356.
[6] R.D. Cortright, R.R. Davda, J.A. Dumesic, Nature 418 (2002) 964–967.
[7] C.T. Au, C.F. Ng, M.S. Liao, Journal of Catalysis 185 (1999) 12–22.
[8] B. Zhang, X. Tang, Y. Li, Y. Xu, International Journal of Hydrogen Energy 32 (13) (2007) 2367–2373.
[9] J.W. Shabaker, G.W. Huber, R.R. Davda, R.D. Cortright, J.A. Dumesic, Catalysis Letters 88 (2003) 1–8.
[10] J.W. Shabaker, G.W. Huber, J.A. Dumesic, Journal of Catalysis 222 (2004) 180–191.
[11] R.R. Davda, J.W. Shabaker, G.W. Huber, R.D. Cortright, J.A. Dumesic, Applied Catalysis B: Environmental 56 (2005) 171–186.
[12] D. Duprez, C. Descorme, T. Birchem, R. Rohart, Topics in Catalysis 16–17 (2001) 49–56.
[13] R.J. Gorte, AiChE Journal 56 (2010) 1126–1135.
[14] E. Mamontov, T. Egami, R. Brezny, M. Koranne, Journal of Physical Chemistry B 104 (2000) 11110–11116.
[15] D. Srinivas, C.V.V. Satyanarayana, H.S. Potdar, P. Ratnasamy, Applied Catalysis A-General 246 (2003) 323–334.
[16] N. Laosiripojana, S. Assabumrungrat, Applied Catalysis B: Environmental 66 (2006) 29–39.
[17] V. Nichele, M. Signoretto, F. Menegazzo, A. Gallo, V. Dal Santo, G. Cruciani, G. Cerrato, Applied Catalysis B: Environmental 111–112 (2012) 225–232.
[18] J. Llorca, N. Homs, P. Ramírez de la Piscina, Journal of Catalysis 227 (2004) 556–560.
[19] J.C. Vargas, S. Libs, A.C. Roger, A. Kiennenman, Catalysis Today 107–108 (2005) 417–425.
[20] F. Romero-Sarria, J.C. Vargas, A.C. Roger, A. Kiennenman, Catalysis Today 133–135 (2008) 149–153.
[21] J.P. Breen, R. Burch, H.M. Coleman, Applied Catalysis B: Environmental 39 (2002) 65–74.
[22] D.K. Liguras, D.I. Kondarides, X.E. Verykios, Applied Catalysis B: Environmental 43 (2003) 345–354.
[23] E.C. Wanat, K. Venkataraman, L.D. Schmidt, Applied Catalysis A-General 276 (2004) 155–162.
[24] H. Idriss, Platinum Metals Review 48 (2004) 105–115.
[25] M. Araque, J.C. Vargas, Y. Zimmermann, A.C. Roger, International Journal of Hydrogen Energy 36 (2) (2011) 1491–1502.
[26] E. Ambroise, C. Courson, A. Kiennenman, A.C. Roger, O. Pajot, E. Samson, G. Blanchard, Topics in Catalysis 52 (2009) 2101–2107.
[27] M. Araque, L.M. Martínez T, J.C. Vargas, M.A. Centeno, A.C. Roger, Applied Catalysis B: Environmental 125 (2012) 556–566.
[28] E. Ambroise, C. Courson, A.C. Roger, A. Kiennenman, G. Blanchard, S. Rousseau, X. Carrier, E. Marceau, C. La Fontaine, F. Villain, Catalysis Today 154 (2010) 133–141.
[29] Y. Madier, C. Descorme, A.M. Le Govic, D. Duprez, Journal of Physical Chemistry B 103 (1999) 10999–11006.
[30] A. Martínez-Arias, M. Fernandez-García, V. Ballesteros, L.N. Salamanca, J.C. Conesa, C. Otero, J. Soria, Langmuir 15 (1999) 4796–4802.
[31] R.D. Shannon, Crystal physics, diffraction, theoretical and general crystallography, Acta Crystallographica Section A (1976) 751.
[32] C. Diagne, H. Idriss, A. Kiennenman, Catalysis Communications 3 (2002) 565–571.
[33] O.H. Laguna, M.A. Centeno, G. Arzamendi, L.M. Gandía, F. Romero-Sarria, J.A. Odriozola, Catalysis Today 157 (2010) 155–169.
[34] J.E. Spanier, R.D. Robinson, F. Zhang, S.W. Chan, I.P. Herman, Physical Review B: Condensed Matter Physics 64 (2001) 2454071–24540713.
[35] L. Cao, L. Pan, C. Ni, Z. Yuan, S. Wang, Fuel Processing Technology 91 (2010) 306–312.
[36] H. Vidal, J. Kaspar, M. Pijolat, G. Colón, S. Bernal, A. Córdon, V. Perrichon, F. Fally, Applied Catalysis B: Environmental 30 (2001) 75–85.
[37] J. Liu, Z. Zhao, J. Wang, C. Xu, A. Duan, G. Jiang, Q. Yang, Applied Catalysis B: Environmental 84 (2008) 185–195.
[38] J. Jiang, L. Li, Materials Letters 61 (2007) 4894–4896.
[39] T. Yamaguchi, N. Ikeda, H. Hattori, K. Tanabe, Journal of Catalysis 67 (1981) 324–330.
[40] S. Damyanova, J.M.C. Bueno, Applied Catalysis A-General 253 (2003) 135–150.
[41] A. Trovarelli, C. Deleitenburg, G. Dolcetti, J.L. Lorca, Journal of Catalysis 151 (1995) 111–120.
[42] A. Trovarelli, Catalysis Reviews: Science and Engineering 38 (1996) 439–520.
[43] E. Aneggi, M. Boaro, C. Leitenburg, G. Dolcetti, A. Trovarelli, Journal of Alloys and Compounds 408–412 (2006) 1096–1102.
[44] A. Trovarelli, F. Zamar, J. Llorca, C. d. Leitenburg, G. Dolcetti, J.T. Kiss, Journal of Catalysis 169 (1997) 490–502.
[45] M.G. Cutrufello, I. Ferino, R. Monaci, E. Rombi, V. Solinas, Topics in Catalysis 19 (2002) 225–240.
[46] G. Jacobs, R.A. Keogh, B.H. Davis, Journal of Catalysis 245 (2007) 326–337.
[47] S.M. Lima, A.M. Silva, U.M. Graham, G. Jacobs, B.H. Davis, L.V. Mattos, F.B. Noronha, Applied Catalysis A-General 352 (2009) 95–113.
[48] J.C. Vargas, E. Vanhaecke, A.C. Roger, A. Kiennemann, Studies in Surface Science and Catalysis 147 (2004) 115–120.
[49] G. Vlaic, R. Di Monte, P. Fornasiero, E. Fonda, J. Kaspar, M. Graziani, Journal of Catalysis 182 (1999) 378–389.
[50] F. Dong, A. Suda, T. Tanabe, Y. Nagai, H. Sobukawa, H. Shinjoh, M. Sugiura, C. Descorme, D. Duprez, Catalysis Today 93–95 (2004) 827–832.
[51] A. Gallo, C. Pirovano, P. Ferrini, M. Marelli, R. Psaro, S. Santangelo, G. Faggio, V. Dal Santo, Applied Catalysis B: Environmental 121–122 (2012) 40–49.
[52] M. Slinn, K. Kendall, C. Mallon, J. Andrews, Bioresource Technology 99 (2008) 5851–5858.
[53] Y. Cui, V. Galvita, L. Rihko-Struckmann, H. Lorenz, K. Sundmacher, Applied Catalysis B: Environmental 90 (2009) 29–37.
[54] V. Chiodo, S. Freni, A. Galvagno, N. Mondello, F. Frusteri, Applied Catalysis A-General 381 (2010) 1–7.
[55] B. Pereira, N. Homs, S. Martí, J.L.G. Fierro, P. Ramírez de la Piscina, Journal of Catalysis 257 (2008) 206–214.
[56] E.B. Pereira, P. Ramirez de la Piscina, S. Marti, N. Homs, Energy & Environmental Science 3 (2010) 487–493.
[57] D.L. Trimm, Catalysis Today 49 (1999) 3–10.
[58] C.H. Bartholomew, Catalysis Reviews 24 (1982) 67–112.
[59] D.L. Trimm, Catalysis Today 37 (1997) 233–238.
[60] J.R. Rostrup-Nielsen, Catalysis Today 37 (1997) 225–232.
[61] L.F. Bobadilla, A. Alvarez, M.I. Dominguez, F. Romero-Sarria, M.A. Centeno, M. Montes, J.A. Odriozola, Applied Catalysis B: Environmental 123–124 (2012) 379–390.
[62] E.A. Sanchez, R.A. Comelli, International Journal of Hydrogen Energy 37 (2012) 14740–14746.
[63] N.F. Brown, M.A. Barteau, Journal of the American Chemical Society 114 (1992) 4258–4265.
[64] J. Barrault, J.M. Clacens, Y. Pouilloux, Topics in Catalysis 27 (2004) 137–142.